Journal of Power Sources 189 (2009) 385–390

Contents lists available at ScienceDirect

Journal of Power Sources

journal homepage: www.elsevier.com/locate/jpowsour

Lithium ion transport pathways in xLiCl–$(1-x)(0.6Li_2O–0.4P_2O_5)$ glasses

R. Prasada Rao*, T.D. Tho, S. Adams

Department of Materials Science and Engineering, National University of Singapore, 117574, Singapore

ARTICLE INFO

Article history:
Received 30 June 2008
Received in revised form 31 July 2008
Accepted 31 July 2008
Available online 15 August 2008

Keywords:
Molecular dynamics simulation
Lithium ion conduction
Bond valence approach
Ion transport in glasses

ABSTRACT

xLiCl–$(1-x)(0.6Li_2O–0.4P_2O_5)$ systems with $x = 0.1, 0.15, 0.2, 0.25$, have been prepared using melt quenching method and their ionic conductivity was characterized by impedance spectroscopy. Molecular dynamics (MD) simulations for the same systems have been performed with an optimized potential, fitted to match bond lengths, coordination numbers and ionic conductivity. Based on the equilibrated configurations of these MD simulations, ion transport pathways are modelled in detail by the bond valence approach to clarify the influence of the halide dopant concentration on the glass structure and its consequence for Li ion mobility. Features of the consequential ion transport pathway models (such as volume fraction and local dimensionality of the percolating pathway) are compared to pathway models for related glassy solid electrolytes based on reverse Monte Carlo modelling of diffraction data.

1. Introduction

Lithium ion-conducting glasses are well known due to their applications in electrochemical devices such as solid-state microbatteries, fuel cells, chemical sensors and smart windows. However mechanism of ionic conductivity in these materials and the effect of halide dopants is still not fully understood.

Structural studies of binary phosphate glasses have been reported using neutron and X-ray diffraction (see reviews by Brow [1] and Hoppe et al. [2]), MD simulations [3–6] and spectroscopic techniques [7]. These binary glasses can be prepared up to 66 mol.% of Li_2O. Glass forming region in ternary glass system $LiPO_3$–LiX [X = I, Br, Cl] has been reported along with their ionic conductivity (σ) [8]. Glasses form up to 30 mol.% of LiCl and 33 mol.% of LiBr and LiI. σ increases with halogen ion size (and polarisability) and with increasing LiX content throughout the glass forming region. Another study [9] in Li_2O–P_2O_5–LiCl system reports glass forming region up to nearly 30 mol.% of LiCl for R ($R = Li_2O/P_2O_5$) varying between 0.67 to 1.38 and up to 35 mol.% for R value of 0.25. The glass transition temperature T_g decreases and σ increases as LiCl content increases for all values of R studied. Conclusions from Raman spectroscopy studies of $0.3LiCl–0.7(0.58Li_2O–0.42P_2O_5)$ glass in the same study indicate that the addition of Li_2O breaks up P–O–P bridges, creating non-bridging oxygens (NBOs) which reduce the lengths of chains formed by P–O–P bridges, while the addition of LiCl does not bring about any such modification of chain lengths in the glass network, though it reduces the T_g of the parent glass. In contrast, IR and XPS studies of $x(2LiCl)y(Li_2O)(100-x-y)P_2O_5$ [$x = 0$, 10, 20, $y = 50$, 60][10] suggest that the more open structure of the halide doped glasses is achieved by Cl^- altering the P–O–P glass network. X-ray diffraction study and MD simulation of $0.52Li_2O–0.48P_2O_5$, $0.45Li_2O–0.42P_2O_5–0.13LiCl$ and $0.39Li_2O–0.36P_2O_5–.25LiCl$ glasses [11,12] reports that the addition of Li_2O to P_2O_5 breaks up the 3D branched structure creating more non-bridging oxygens and the addition of LiCl makes the structure less rigid and creates wider channels for Li^+ movement, thus enhancing σ and decreasing T_g. Further structural reports for Li_2O–P_2O_5–LiCl glass [7,13] confirm that no P–Cl bonds are formed and that LiCl dissolves interstitially in $LiPO_3$ glass network. While Raman, IR spectroscopy and Reverse Monte Carlo fits of diffraction data accordingly find that LiCl acts as a dopant only in lithium borate glasses [14,15]; in Li_2O–TeO_2–LiCl glasses [16,17], the addition of LiCl is reported to produce NBOs leading to the formation of Te–Cl bonds in the equatorial position of the trigonal pyramid TeO_4 unit. ^{7}Li MAS NMR studies of LiCl–Li_2O–P_2O_3 suggest the existence of LiCl aggregates for high LiCl contents close to the limit of the glass forming region, and it is concluded that these lead to the high mobility of Li^+ ion [18]. Yet another impedance spectroscopy study of Li_2X–B_2O_3–SiO_2 (X = O, Cl_2) [19] concludes that the network dilatation brought about by the addition of Cl^- has little influence on conductivity.

In order to further understand the relation between pathway volume of mobile Li^+ ion and the influence of LiCl content in xLiCl–$(1-x)(0.6Li_2O–0.4P_2O_5)$ (where $x = 0.1, 0.15, 0.20, 0.25$) glass preparation and bond valence approach was applied for the MD simulated glasses here.

* Corresponding author. Tel.: +65 6516 7898; fax: +65 6776 3604.
E-mail address: mserpr@nus.edu.sg (R. Prasada Rao).

0378-7753/$ – see front matter © 2008 Elsevier B.V. All rights reserved.
doi:10.1016/j.jpowsour.2008.07.089

2. Methodology

2.1. Sample preparation and properties characterization

Ternary glasses xLiCl–$(1-x)(0.6Li_2O–0.4P_2O_5)$ (where $x = 0.1$, 0.15, 0.20, 0.25) were prepared by the conventional melt quenching method [10] using $NH_4H_2PO_4$, Li_2CO_3 and LiCl. Due to the hygroscopic nature of phosphate glasses the samples were stored in a desiccator with silica. It was noticed that LiCl partially evaporates during preparation and the amount of Cl^- present in the glass therefore to find the exact composition of the prepared sample we used Scanning Electron Microscopy (SEM) with the aid of Energy Dispersive X-ray Detection (EDX). Table 1 shows a comparison between the expected and observed chloride contents in the corresponding glasses. Hereafter experimental data will refer to the observed compositions. MD simulations are conducted for the expected compostions.

The quenched samples were characterized by X-ray powder diffractometry using Cu Kα radiation (PANalytical X'Pert PRO) equipped with a fast linear detector (X'Celerator), which can collect 100 steps at the same time. XRD data were collected in the 2θ range 10–110° with a nominal scan rate of 70 s step^{-1} and a step size of 0.05° at room temperature. No sharp Bragge peaks were observed. It conforms glassy nature of the samples. Density of glasses was measured by Archimedes' principle (Density Determination Kit Mettler ME-33360) using toluene as the immersion liquid. The glass transition temperature, T_g was determined using Differential Scanning Calorimetry (DSC; *TA Instruments 2920 Modulated DSC*) at a heating rate of 10 K min^{-1} under constant flow of high purity N_2 gas.

Ionic conductivity measurements at different temperatures were carried out by impedance spectroscopy (*Schlumberger Solartron SI 1260*) in the frequency range of 1 Hz to 1 MHz. Commercially available silver paint (ion-blocking electrode) was applied on both sides of the glass sample to achieve a controlled contact area for the ionic conductivity determination. The sample was kept in a Kiel-type Electrochemical Cell (Ionic Systems). At each temperature the sample was kept for 10 min for thermal equilibration. The bulk resistance R_b was determined from fitting impedance data to Nyquist plots ($-Z''$ versus Z'). The equivalent circuit consists of C_b, R_b and CPE, where C_b is the geometric capacitor between the electrodes, and CPE is the constant phase element due to the polarisation distribution at the interface between blocking electrodes and glass.

2.2. Computer simulations

Constant volume (NVT) MD simulations have been performed on structure models of $(1-x)(0.6Li_2O–0.4P_2O_5)$–$x$LiCl glasses (where $x = 0.10$, 0.15, 0.20, 0.25). The volume of the simulation box is derived from our density determinations (Fig. 2). The optimized potential parameters shown in Tables 2 and 3 have been derived in the frame of this project by fitting to experimentally known bond lengths and coordination numbers.

Starting at a temperature of 1500 K, the system containing 1975–2170 atoms was cooled by scaling velocities to 1000, 700, 500, 400 K and finally cooled to 300 K with a time step of 2 fs. At 1500, 1000 and 700 K, equilibration time was 300 ps followed by a NVT simulation (Hoover thermostat) for 200 ps. At 500, 400, 300 K the equilibration time was increased to 600 ps and the production run after equilibration was also increased to 400 ps. Thus the calculation of mean square displacement (MSD) for all atoms was based on the final 200 ps at 1500, 1000, 700 K, and the final 400 ps for the temperatures 500, 400 and 300 K below the glass transition temperature. Besides the Coulomb interactions the forcefield involves a Born repulsion term (Buckingham potential with $C_{ij} = 0$) and a Vessal-type three-body term as follows:

$$\phi_{ij} = \frac{Z_i Z_j e^2}{r_{ij}} + A_{ij}\exp\left(\frac{-r_{ij}}{\rho_{ij0}}\right) + \frac{k_{ij}}{8(\theta_{jik}-\pi)}\{[(\theta_0-\pi)^2-(\theta_{jik}-\pi)^2]^2\}\exp\left[-\frac{r_{ij}}{\rho_{ij}}-\frac{r_{jk}}{\rho_{jk}}\right]$$

Here ϕ_{ij} is the potential function between particles i and j, Z_i is the effective atomic charge of atom i, θ_0 is the equilibrium angle subtended by r_{ij} and r_{ik}. A_{ij}, ρ_{ij0}, k_{ij} and ρ_{ij} are forcefield parameters. The ionic charges used in MD simulations for Li, Si, P, O, Cl are +0.6e, +2.4e, +3e, −1.2e, −0.6e, respectively. Fig. 1 shows the pair correlation function (PCF) and Running coordination (RCN) for $x = 0.25$ glass, indicating the presence of PO_4 tetrahedra. Bond

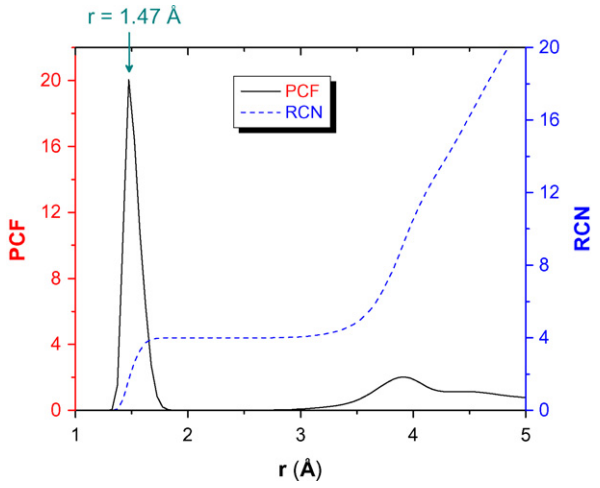

Fig. 1. PCF and RCN of P–O for $0.45Li_2O–0.30P_2O_5–0.25$LiCl glass.

Table 1
Chloride content (wt%) in the studied $(1-x)(0.6Li_2O–0.4P_2O_5)$–$x$LiCl glasses

Nominal glass composition	Theoretical wt_{Cl}%	Experimental wt_{Cl}%
$0.54Li_2O–0.36P_2O_5–0.10$LiCl	4.96	4.87
$0.51Li_2O–0.34P_2O_5–0.15$LiCl	7.61	7.14
$0.48Li_2O–0.32P_2O_5–0.20$LiCl	10.39	10.26
$0.45Li_2O–0.30P_2O_5–0.25$LiCl	13.30	13.20

Table 2
Optimized two-body potential parameters for LiCl doped phosphate glasses

Interaction (i–j)	A_{ij} (eV)	ρ_{ij0} (Å)
P–O	2900.57	0.212
O–O	2100.43	0.295
Li–O	25500.42	0.170
Li–Cl	150000.00	0.176
P–Cl	2500.00	0.450
Cl–Cl	1500.00	0.60

Table 3
Potential parameters for the three-body Vessal term in the forcefield for LiCl doped phosphate glasses

Interaction (i–j–k)	O–P–O
k (eV)	0.0129
θ_0	103°
ρ_{ij} (Å)	0.2252
ρ_{ik} (Å)	0.1191
r_c^* (Å)	1.90

r_c^*: cut-off in r_{ij} and r_{jk}.

valence analysis is applied to the final configuration obtained at 300 K.

2.3. Bond valence approach

Empirical relationships between bond length and bond valence (BV) are widely used to identify plausible equilibrium sites for an atom in a crystal structure as sites where the BV sum of the atom matches its oxidation sate [20]. A modification of the BV approach that improves the assessment of non-equilibrium site energies by a systematic adjustment of BV parameters to the bond softness [21–26] extends the application range of this simple tool to structure–property relationship studies in solid electrolytes. For that purpose, 'accessible' sites for a mobile ion, A, in a local structure model are identified using empirical relationships between the bond length, R and a so-called bond valence, s_{A-X},

$$s_{A-X} = \exp\left[\frac{(R_0 - R)}{b}\right]$$

as sites where the mismatch of the bond valence sum, $V(A)$

$$|\Delta V(A)| = |\sum_X s_{A-X} - V_{id}(A)| + \sum_X p_{A-X}$$

over the s_{A-X} from all adjacent counterions, X approaches the ideal valence, $V_{id}(A)$ (which equals its oxidation state). To enhance the chemical plausibility of BV mismatch 'energy landscapes', $|\Delta V(A)|$ contains a penalty function, p_{A-X}, that discriminates against sites where a matching $V(A)$ is achieved by unfavourable strongly asymmetric coordinations [24] and is complemented by hard minimum distance and soft coordination number constraints. In contrast to most conventional BV parameter sets our *softBV* parameters are based on the assumption that not only the counterions of the first coordination shell but all counterions up to a cut-off radius of 4–8 Å (depending on sizes and polarisabilities of the ions involved) contribute to $V(A)$. This is indispensable for modelling ion transport pathways as it avoids artefacts in the BV sum variation, when an ion moves across the border of its coordination shell. BV ion transport pathway models are based on the supposition that paths between accessible sites, along which $|\Delta V(A)|$ remains sufficiently low represent probable ion transport paths. Isosurfaces of fixed maximum BV sum mismatch $|\Delta V(A)|$ for a certain ion type A will thus enclose regions that an A ion in the pathway may reach with a certain activation energy, E_a. Low BV mismatch regions that include both occupied and vacant sites, therefore, enable local jumps of A. A long-range transport requires pathways that extend through the whole structure. For periodic models this is equivalent to spanning the model box. Determining the 'pathway volume' for a given maximum value of $|\Delta V(A)|$ yields a simple and reliable way of characterizing ion transport pathways in local structure models of disordered systems [23,25]. To evaluate this pathway volume, $V(A)$, has to be calculated for a hypothetical A^+ ion at each point in the structure. In practice, the structure model is divided into a primitive grid containing ~3.3 million cubic volume elements with a size of ca. $(0.2\,Å)^3$, i.e. about 1600 volume elements per atom. A volume element is considered to belong to the conduction pathway if $|V(A) - V(A)_{ideal}|$ is below a fixed threshold value or if the sign of $(V - V_{ideal})$ alters within the volume element (the second condition cushions effects of the limited grid resolution). Accessible volume elements that share common faces or edges belong to the same 'pathway cluster'. It is assumed that these pathway clusters contribute to dc conductivity only if they percolate through the structure model. The volume fraction, F, of the percolating pathways turns out to be a suitable measure of E_a and thereby (in the case of glasses) also of the room temperature conductivity. The remaining restricted pathway clusters are considered to contribute only to ac conductivity. As mentioned above, the threshold value for $|\Delta V(A)|$ has to be chosen somewhat arbitrarily. When comparing pathways for different types of mobile ions, we find that the most suitable value will, as discussed further below, depend on the mass, m_A, of the mobile ion.

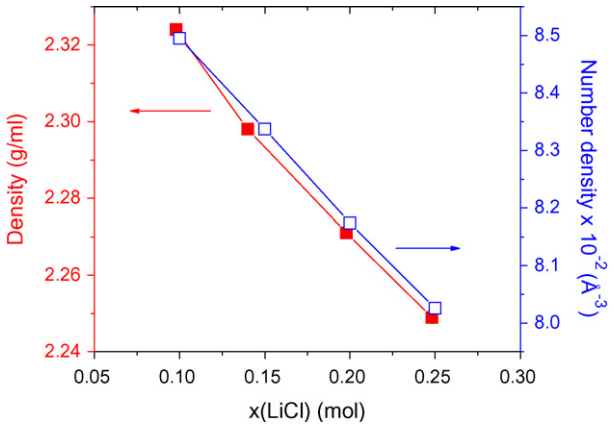

Fig. 2. Composition dependence of the mass density (solid symbols) and number density (open symbols) in the glasses of $(1-x)(0.6Li_2O–0.4P_2O_5)$–$x$LiCl. The lines are drawn as a guide to the eye.

3. Results and discussions

Both measured density and number density of glasses are decreasing with increase of LiCl content (Fig. 2). This indicates that the glass network is becoming more open which leads to the decrease of T_g (Fig. 3) and an increase of Li^+ ion mobility. Complex impedance measurements of the glasses were carried out from 27 to 100 °C. The Nyquist plots were fitted by using an equivalent circuit model of one RC couple (representing the bulk resistance and geometric capacitance) in series with one CPE (representing polarisation at the electrode: electrolyte interface) (Fig. 4). A series of Nyquist plots of $0.54Li_2O–0.36P_2O_5–0.10$LiCl glass at different temperatures is shown in Figs. 4 and 5 shows the Arrhenius behaviour of dc ionic conductivity as expected. Table 4 shows the experimental and MD ionic conductivity and at 27 °C. Comparison of ionic conductivity of both experimental and simulations is shown in Fig. 6. MD values are of the same order of the experimental values. The

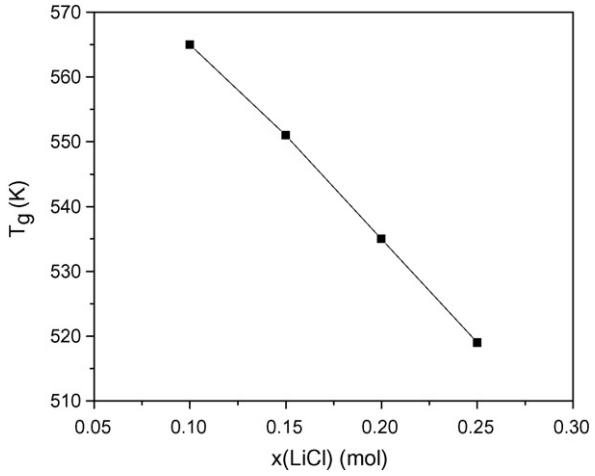

Fig. 3. Composition dependence of the glass transition temperature (T_g) in the glasses of $(1-x)(0.6Li_2O–0.4P_2O_5)$–$x$LiCl.

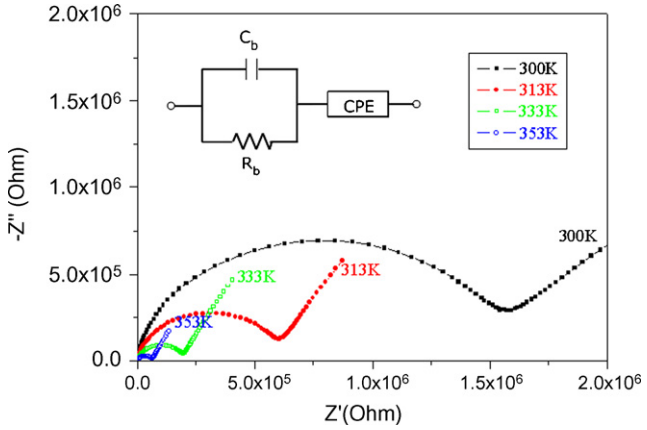

Fig. 4. Nyquist plots of $0.54Li_2O–0.36P_2O_5–0.10LiCl$ glass at different temperatures and equivalent circuit used for impedance fitting.

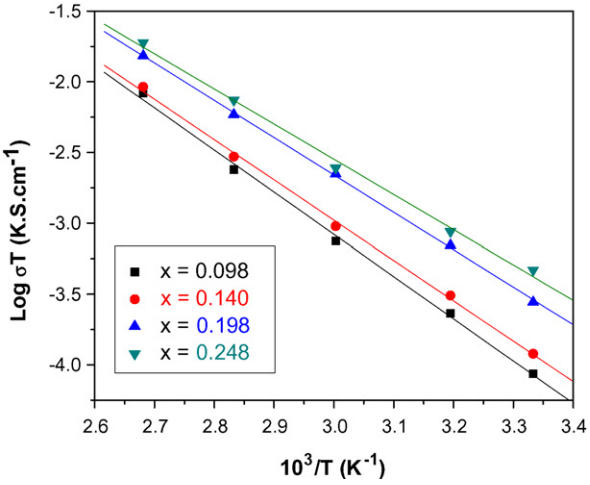

Fig. 5. Arrhenius plots of the dc conductivities obtained from impedance spectroscopy for different glasses.

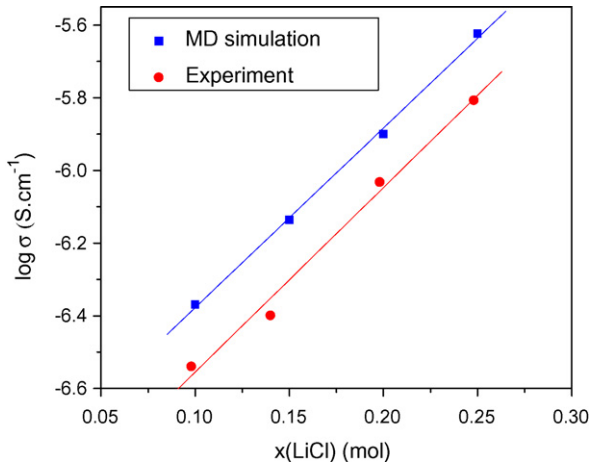

Fig. 6. Comparison of ionic conductivities for $(1-x)(0.6Li_2O–0.4P_2O_5)–xLiCl$ glasses with composition at 27 °C. The lines are linear fits of data.

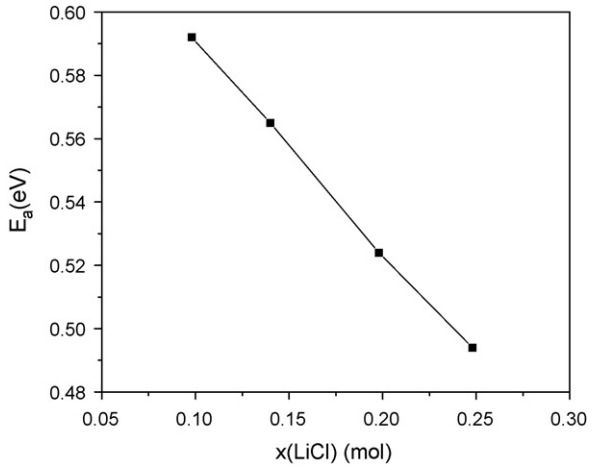

Fig. 7. Composition dependence of activation energy (E_a) in the glass series $(1-x)(0.6Li_2O–0.4P_2O_5)–xLiCl$.

trend of increment of conductivity is same in both cases. The slope of Arrhenius plots decreases with increase of LiCl, consequently activation energy (E_a) decreases form 0.494 eV (47.6 kJ mol^{-1}) to $x = 0.25$ (Fig. 7).

Fig. 8 shows the presence of PO_4 tetrahedra in MD generated configuration of $0.45Li_2O–0.30P_2O_5–0.25LiCl$ glass at 300 K. Final equilibrated MD configurations glasses were used for bond valence analysis. The threshold value for $|\Delta V(A)|$ is chosen to be 0.10 valence units to allow for a comparison with existing reference data for a wide range of other oxide glasses. Using the bond valence approach it can be investigated whether the Li^+ ions form LiCl clusters in the investigated glass structures, as had been discussed previously in the literature for related systems [24]. It is found that this hypothesis can be ruled out for the system under study: the distribution of relative contributions of Li–Cl bonds to the Lithium BV sums in these glasses (cf. Fig. 9) demonstrates that, as to be expected for a modified random network glass, only a small fraction of the Li atoms are bonded predominantly by chloride ions (<2% for all glasses). For none of the Li atoms in these glasses the coordination polyhedron exists exclusively of Cl^- ions. More than 95% oxide contribution occurs for 20% ($x = 0.25$; O:Cl ratio 7.8:1) to 64% ($x = 0.10$, O:Cl ratio 23.4:1) of the Li atoms. This also clarifies that any lithium ion transport pathway has to run along sites with mixed oxide/halide or exclusive oxide coordination. Fig. 10 shows the local environment of the Li^+ ion sites located in the conduction pathways of glasses under present investigation. The density of pathways slightly increases with increasing chloride content from $x = 0.10$ to 0.25 (the volume fraction of percolating pathways (F) increases from 5.4% to 5.8%), in line with the increase of ionic conductivity in these glasses, except at $x = 0.15$. Figs. 11 and 12 relate the volume fraction of the percolating ion conduction pathways in

Table 4
MD and experimental ionic conductivities for $xLiCl–(1-x)(0.6Li_2O–0.4P_2O_5)$ glasses with nominal and experimental compositions at 27 °C

Nominal glass composition	σ_{MD} (σ_{exp}) (S cm^{-1})	Experimental glass composition
$0.54Li_2O–0.36P_2O_5–0.10LiCl$	4.28×10^{-7} (2.89×10^{-7})	$0.54Li_2O–0.36P_2O_5–0.098LiCl$
$0.51Li_2O–0.34P_2O_5–0.15LiCl$	7.32×10^{-7} (3.99×10^{-7})	$0.51Li_2O–0.34P_2O_5–0.141LiCl$
$0.48Li_2O–0.32P_2O_5–0.20LiCl$	1.26×10^{-6} (0.93×10^{-6})	$0.48Li_2O–0.32P_2O_5–0.198LiCl$
$0.45Li_2O–0.30P_2O_5–0.25LiCl$	2.38×10^{-6} (1.56×10^{-6})	$0.45Li_2O–0.30P_2O_5–0.248LiCl$

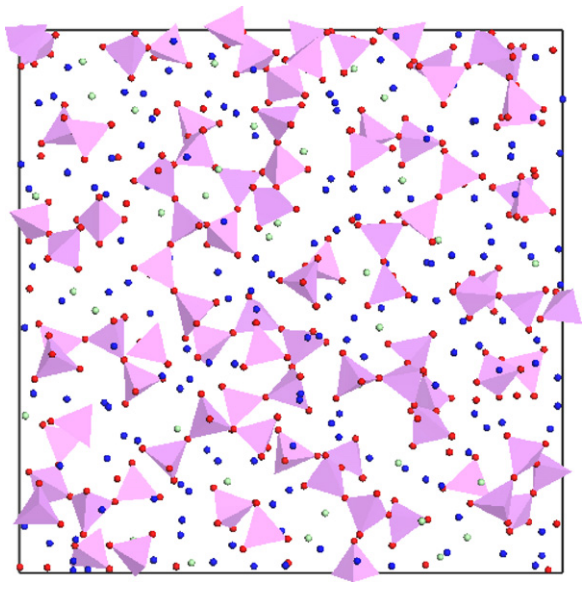

Fig. 8. Structure of $0.45Li_2O–0.30P_2O_5–0.25LiCl$ glass at 300 K. Oxide atoms (red spheres) are around P (shown as tetrahedra), Li: blue spheres, Cl: green spheres. Only 1/4 of the structure model is shown along z (perpendicular to the plane of view) to reduce overlap. (For interpretation of the references to color in this figure legend, the reader is referred to the web version of the article.)

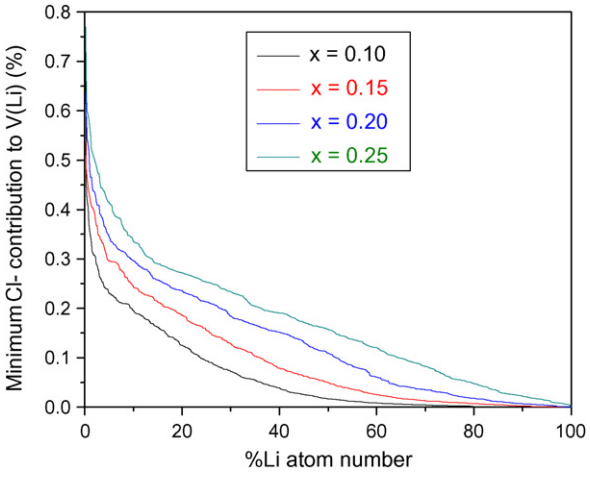

Fig. 9. Distribution of relative contributions of Li–Cl bonds to the BV sums of Li^+ ions in the glasses $(1-x)(0.6Li_2O–0.4P_2O_5)–xLiCl$ for $x = 0.10–0.25$. For the case $x = 0.25$ only 10% of the Li experience a BV contribution exceeding 34%.

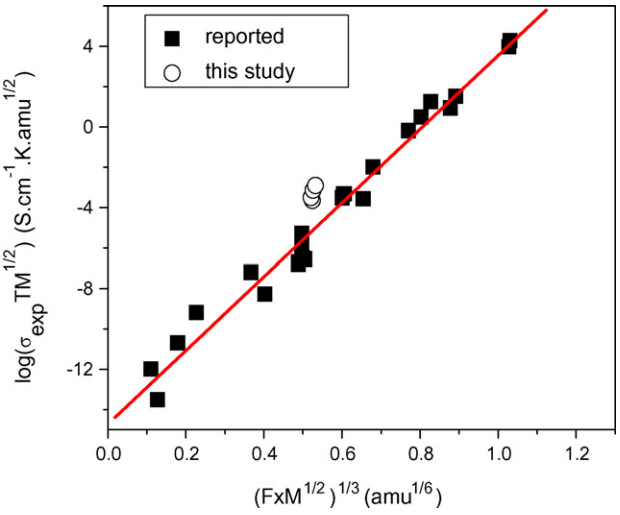

Fig. 11. Variation of pathway volume fraction of Li^+ ion with experimental room temperature ionic conductivity. Data in solid symbol refer to data from RMC models [23]. Data in open circles refer to MD simulated structures of $(1-x)(0.6Li_2O–0.4P_2O_5)–xLiCl$ glasses (where $x = 0.10$, 0.15, 0.20 and 0.25).

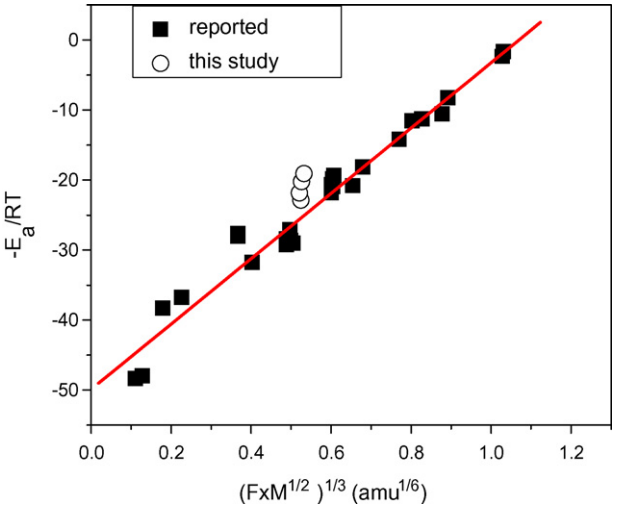

Fig. 12. Variation of pathway volume fraction of Li^+ ion with activation energy. Data in solid symbol refer to data from RMC models [23]. Data in open circles refer to MD simulated structures of $(1-x)(0.6Li_2O–0.4P_2O_5)–xLiCl$ glasses (where $x = 0.10$, 0.15, 0.20 and 0.25).

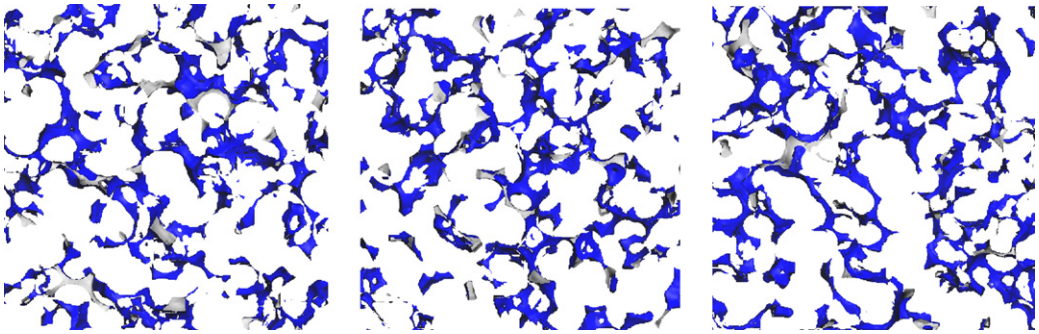

Fig. 10. Slices of the isosurfaces of constant lithium bond valence sum mismatch $|\Delta V(Li)|$ in the glasses $(1-x)(0.6Li_2O–0.4P_2O_5)–xLiCl$ for $x = 0.15$, 0.20, 0.25 (left to right) at 300 K, projected along the z-axis.

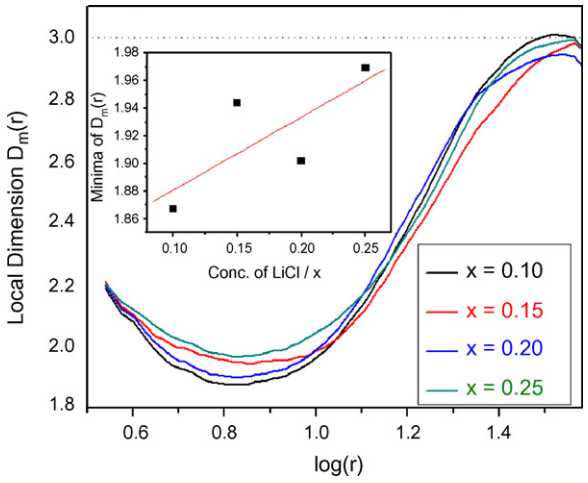

Fig. 13. The local Li^+ ion transport pathway dimension, $D_m(r)$ vs. radius (r) for $(1-x)(0.6Li_2O–0.4P_2O_5)$–$x$LiCl glasses. Inside graph indicates the variation of local dimensional minima with respect to LiCl variation.

the investigated glasses to their experimentally observed absolute values of the ionic conductivity and activation energy (E_a). Results of the present MD study are compared with the previously reported RMC values. As seen from Figs. 11 and 12, the increase in the volume fraction when we move from the glass $x = 0.1$ to 0.25 leads to an increase in the ionic conductivity and a corresponding decrease in the activation energy, except for $x = 0.15$. Using the concept of mass-radius dimension [14], we can further investigate details of the pathway structure. As seen from Fig. 13, the minimum value of local pathway dimension increases with the LiCl content, again except for $x = 0.15$. This minimum value of local dimension may be largely thought of as characterizing the width of the Li ion transport pathway at the bottleneck of elementary transport steps. Thus the increase of the local pathway dimension as a result of doping by the more polarisable Cl^- ion indicates that channels accessible for Li^+ ion movement are widened by the doping. This contributes to the decrease of activation energy and increase of ionic conductivity and with rising LiCl content.

4. Concluding remarks

Optimized potential parameters reproduce the reported bond lengths and coordinations. Moreover, experimental and simulated values of the ionic conductivity are well in agreement. The effect of LiCl addition on the pathways for the mobility of Li^+ ions is quantified for the phosphate glasses xLiCl–$(1-x)$ $(0.6Li_2O–0.4P_2O_5)$. Pathway volume fraction for Li ion transport and experimental conductivities accordingly exhibit an unusually small effect of halide doping on the conductivity. For the investigated compositions ion transport cannot be related to (previously postulated) LiCl aggregates as such aggregates do not exist—at least in the simulated structures. Nearly all Li have a mixed oxide chloride coordination. The minimum value of local pathway dimension increases with the LiCl content, except for $x = 0.15$. The higher minimum value of local dimension means the Li ion transport pathway is more open, i.e. channels for the Li ion movement become wider.

References

[1] R.K. Brow, J. Non Cryst. Solids 263/264 (2000) 1–28.
[2] U. Hoppe, G. Walter, R. Kranold, D. Stachel, J. Non Cryst. Solids 263/264 (2000) 29–47.
[3] A. Karthikeyan, P. Vinatier, A. Levasseur, K.J. Rao, J. Phys. Chem. B 103 (1999) 6185–6192.
[4] J.-J. Liang, R.T. Cygan, T.M. Alam, J. Non Cryst. Solids 263/264 (2000) 167–179.
[5] T.M. Alam, J.-J. Liang, R.T. Cygan, Phys. Chem. Chem. Phys. 2 (2000) 4427–4432.
[6] R.K. Sistla, M. Seshasayee, J. Non Cryst. Solids 349 (2004) 22–29.
[7] M. Tatsumisago, Y. Kowada, T. Minami, Phys. Chem. Glasses 29 (2) (1988) 63–70.
[8] J.P. Malugani, G. Robert, Mater. Res. Bull. 14 (1979) 1075–1081.
[9] M. Doreau, A. Abou El Anouar, G. Robert, Mater. Res. Bull. 15 (1980) 285–294.
[10] M. Horiuchi, T. Sei, T. Tsuchiya, J. Non-Cryst. Solids 177 (1994) 236–241.
[11] K. Muruganandam, M. Seshasayee, S. Patnaik, Solid State Ionics 89 (1996) 313–319.
[12] R. Prasada Rao, M. Seshasayee, Solid State Commun. 131 (8) (2004) 537–542.
[13] H.L. Tuller, D.P. Button, D.R. Uhlmann, J. Non-Cryst. Solids 40 (1980) 93–118.
[14] A. Hall, S. Adams, J. Swenson, Phys. Rev. B 74 (2006) 174205–174211.
[15] K. Tanaka, T. Yoko, H. Yamada, K. Kamiya, J. Non-Cryst. Solids 103 (1988) 250–256.
[16] Y. Iwadate, H. Kenmotsu, T. Hattori, S. Nishiyama, K. Fukushima, N. Umeshki, T. Nakazawa, K. Noda, J. Alloys Compd. 305 (2000) 130–135.
[17] M. Irion, M. Couzi, A. Levasseur, J.M. Reau, J.C. Brethous, J. Solid State Chem. 31 (1980) 285–294.
[18] Y. Ogiwara, K. Echigo, M. Hayana, J. Non Cryst. Solids 352 (2006) 5192–5198.
[19] W. Muller, D. Kruschke, M. Torge, A. Grimmer, Solid State Ionics 23 (1987) 53–58.
[20] I.D. Brown, The Chemical Bond in Inorganic Chemistry the Band Valence Model, Oxford University Press, New York, 2002.
[21] S. Adams, Acta Crystallogr. B, Struct. Sci. 57 (2001) 278–287.
[22] S. Adams, softBV web pages: http://www.softBV.net, 2003.
[23] S. Adams, J. Swenson, Solid State Ionics 175 (2004) 665–669.
[24] S. Adams, Bull. Mater. Sci. 29 (6) (2006) 1–7.
[25] S. Adams, J. Swenson, Phys. Chem. Chem. Phys. 4 (2002) 3179–3184.
[26] S. Adams, J. Swenson, Solid State Ionics 154/155 (2002) 151–159.